lubricants

MDPI

Article

Analysis of Temperature Characteristics of Double-Row Spherical Roller Bearings Based on CFD

Chengguo Fu [1,2,*], Ting Chen [2], Hui Yang [2], Haibo Li [2], Yuhao Li [3], Yaqi Zhang [2], Weiwei He [2] and Hongbin Cong [4]

[1] School of Mechanical Engineering, Guizhou University of Engineering Science, Bijie 551700, China
[2] School of Mechanical and Electrical Engineering, Henan Institute of Science and Technology, Xinxiang 453003, China; chenting_future@163.com (T.C.); abcyah@163.com (H.Y.); skyseal@126.com (H.L.); zhangyaqi_1988@163.com (Y.Z.); wei989926@163.com (W.H.)
[3] College of Engineering, South China Agricultural University, Guangzhou 510642, China; lyvhao@163.com
[4] Ministry of Agriculture and Rural Affairs, Academy of Agricultural Planning and Engineering, Beijing 100125, China; dabinc123@163.com
* Correspondence: scu_fcg@163.com; Tel.: +86-182-3878-9201

Abstract: Double-row spherical roller bearings are frequently employed as supporting components in mining machinery. In practice, these bearings are lubricated manually, and the bearing chamber is filled with grease, which can lead to issues such as grease wastage and increased bearing temperatures. Additionally, factors such as load and speed also influence the bearing temperature, collectively contributing to inadequate lubrication and potential bearing failure. Consequently, it is essential to investigate the temperature of the bearing under operating conditions. Utilizing tribology theory and the principles of bearing heat generation, a numerical model of fluid–structure interaction heat transmission within the bearing was developed, and finite element analysis was conducted through the ANSYS-Fluent module. The model was verified, and the temperature field of the bearing under varying operating conditions was studied. The findings of this research are as follows: (1) The numerical model demonstrates high accuracy, with a relative error of less than 5% when comparing the experimental temperature values of the jaw crusher bearing to the simulated values. (2) Under diverse operating conditions, the inner ring of the bearing has the highest temperature of all parts of the bearing, while the bearing cavity's flow field has the lowest temperature. (3) The average temperature amplitude across different areas of the bearing system will rise as a result of increases in radial load or the bearing rotational speed. (4) When the grease filling volume increases from minimal to maximal, the average temperature in each bearing area initially decreases before subsequently rising, with the optimal grease filling amount identified as 60%. In operational scenarios, if the bearing temperature exceeds 70 °C, it is imperative to shut down the machine immediately to avert bearing failure. This study on bearing lubrication has practical guiding significance.

Keywords: double-row spherical roller bearings; grease lubrication; fluid–structure interaction heat transfer; temperature characteristics; CFD simulation

check for updates

Received: 8 November 2024
Revised: 13 February 2025
Accepted: 14 February 2025
Published: 15 February 2025

Citation: Fu, C.; Chen, T.; Yang, H.; Li, H.; Li, Y.; Zhang, Y.; He, W.; Cong, H. Analysis of Temperature Characteristics of Double-Row Spherical Roller Bearings Based on CFD. *Lubricants* **2025**, *13*, 85. https://doi.org/10.3390/lubricants13020085

Copyright: © 2025 by the authors. Licensee MDPI, Basel, Switzerland. This article is an open access article distributed under the terms and conditions of the Creative Commons Attribution (CC BY) license (https://creativecommons.org/licenses/by/4.0/).

1. Introduction

Double-row spherical roller bearings play a vital role in the effective operation of mining equipment. Proper lubrication is essential to maintain optimal operating conditions for these bearings, as it minimizes wear and prevents temperature increases, thereby reducing the likelihood of bearing failures [1,2]. Studies indicate that approximately

80% of bearing damage can be attributed to poor lubrication, which mainly includes insufficient lubricating grease and grease oxidation and deterioration. The oxidation of lubricating grease during bearing operation is influenced by factors like rotational speed, load, and frictional heat generation [3]. It has been proved that temperature is related to the oxidation rate of lubricating grease. For every 10 °C rise in temperature, the oxidation rate of lubricating grease increases by 1.5- to 2-times, leading to a five-fold reduction in the lifespan of the grease. Meanwhile, the performance of lubricating grease [4,5] holds significant value for the longevity of bearings. Poor lubrication of bearings will lead to severe friction, causing a temperature rise that can lead to bearing failure [6–9]. Consequently, investigating how bearing load, speed, and the filling volume of grease influence the temperature distribution in bearings holds significant practical relevance.

Scholars have extensively researched the temperature field of bearings [10–19]. An analytical model relying on fluid–structure interaction (FSI) heat transfer theory for all-ceramic ball bearings was created by Sun et al. [20]. They investigated the temperature distribution under varying operating conditions. They observed that the temperature in the full ceramic ball bearing is directly related to the speed and load. Li et al. [21] researched the temperature field of angular contact ball bearings and established its computational fluid dynamics (CFD) model. They analyzed the temperature field of the bearings, validated the simulation accuracy through temperature rise experiments, and investigated the impact of lubrication parameters, various working circumstances as well as material types of rolling elements on the bearings' temperature characteristics. Employing the finite element method (FEM), Li et al. [22] explored the effects of different operational parameters on friction power loss. The distribution of temperature, whether in steady state or transient, within high-speed rolling bearings was studied, and the highest temperature was observed on the inner ring raceway, which was aligned with the experimental results from a bearing temperature test. The influence of the airflow velocity and rotating speed on the rolling bearings' operating thermal level was investigated by Sun et al. [23]. The bearings' temperature field was simulated using Fluent software, and the findings indicated a specific correlation between the bearings' maximum temperature and their rotational speed. Based on FSI heat transfer theory, Ma et al. [24] constructed a numerical computational model for high-speed rolling bearings. They examined the correlation between lubrication parameters and thermal equilibrium, revealing a linear increase in temperature with bearing speed. The research revealed that the bearing's outer ring temperature first rises, subsequently falls, and then rises again with an increased supply of oil and the lubricating oil's viscosity. The above research proves that the finite element simulation method can be used to effectively analyze various bearings, enabling the simulation of various test scenarios and significantly reducing testing costs.

At present, the research on double-row spherical roller bearings for mining is relatively limited (bearing working conditions are complex), mainly focusing on experimental research. The use of traditional experimental methods can only obtain macroscopic indicators (service life, the temperature of measurement points, etc.), and there are few research parameters; it is difficult to measure the temperature of the internal area of the bearing through experiments alone, and the internal temperature can only be roughly inferred through the temperature of the measurement point, resulting in large errors in bearing temperature field analysis. However, the finite element method can obtain the temperature of each area inside the bearing. The finite element method is organically combined with experimental verification. After the simulation model is verified, the error between the actual value and the simulated value is small, and the validity of the simulation model can be proved. Therefore, by combining the two, a connection can be established between the temperature at the actual external measurement points and the temperature values of each

part inside the bearing (simulated temperature field). By monitoring the temperature at the external measurement points, the internal state of the bearing (whether it is in good condition or has a fault) can be judged. This method can accurately determine the temperature distribution of each component of the bearing, gain an in-depth understanding of its internal thermal state, establish a connection between the external temperature measurement point of the bearing and the internal temperature, and further optimize the working conditions and lubrication conditions of the bearings. This method not only provides a theoretical reference for improving the service life of bearings but also provides guidance for its practical application.

Consequently, this study focuses on double-row spherical roller bearings as the subject of investigation and adopts the holistic thermogenic approach. To establish the bearing's heat generation model, we calculate its frictional power heat generation under various radial loads, different bearing speeds, and varying lubricating grease filling conditions. After heat transfer, thermal equilibrium is achieved. Utilizing the ANSYS-Fluent module to perform temperature field simulations, the temperature characteristics of the entire bearing system in various areas under operating conditions can be obtained.

2. CFD Calculation Method

The CFD method [25–28] has been extensively utilized in bearing thermal analysis. The process involves establishing the bearing's geometric model and creating and meshing an FSI thermal transfer model for the bearing assembly to analyze the temperature characteristics belonging to double-row spherical roller bearings. Subsequently, the CFD calculation model of bearings needs to be studied, encompassing the kinematic relationship of bearings, the heat generation, and the heat transfer mathematical model, which, along with the heat allocation, function as boundary conditions for input. Finally, the partitioned mesh model is entered into the ANSYS-Fluent module, and the boundary conditions are input into the software for fluid–solid coupling heat transfer calculation to obtain CFD calculation results.

2.1. Modeling

2.1.1. Geometric Model of Bearings

The PE series jaw crushers produced by Henan Wanshi Hengtong Intelligent Equipment Co., Ltd., Xinxiang, China, are widely used in mining machinery. The jaw crusher is driven by an electric motor to drive the belt and belt pulley, which are moved by an eccentric shaft. The specific study focuses on the bearings (model: 22322) at the fixed motor driveshaft, as depicted in Figure 1.

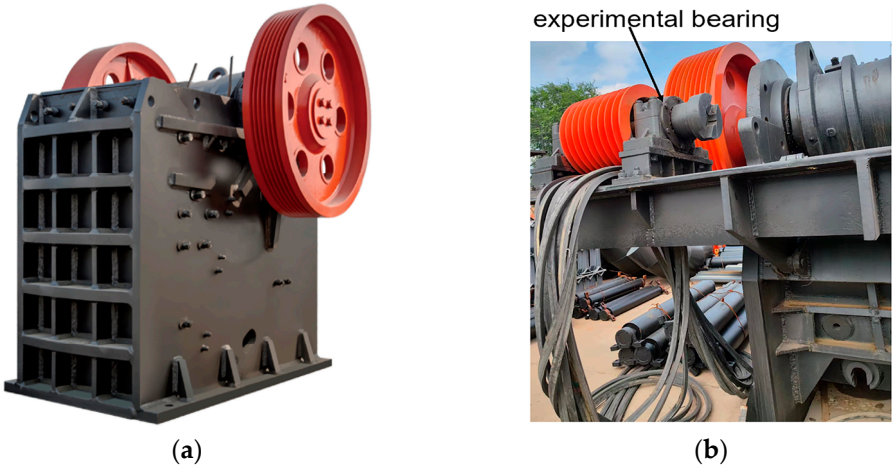
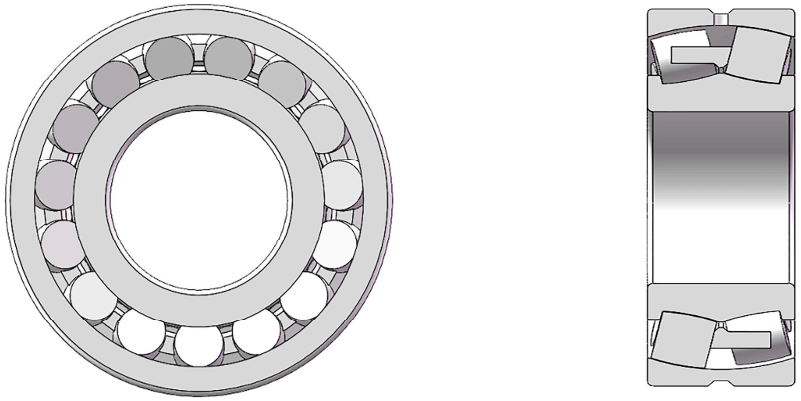


Figure 1. Jaw crusher. (**a**) Overall view. (**b**) Partial view.

The structural parameters for the bearing are listed in Table 1, and the three-dimensional geometric model is illustrated in Figure 2.

Table 1. Double-row spherical roller bearing structural parameters.

Structural Parameters	Parameter Value
Outer diameter D (mm)	240
Inner diameter d (mm)	110
Width B (mm)	80
Pitch diameter d_m (mm)	175
Number of rolling elements Z	30
Rolling elements diameter D_b (mm)	30
Number of rolling elements rows	2
Contact angle α	10°



(**a**) (**b**)

Figure 2. Three-dimensional geometric model of bearings. (**a**) Bearing front view. (**b**) Bearing cross-section.

2.1.2. Establishment and Meshing of Bearing Fluid–Structure Interaction Heat Transfer Numerical Model

The bearing's temperature field results from reaching a thermal equilibrium between heat generation and heat transfer. To analyze friction loss, heat conduction, and heat convection between the domains of solid and fluid, it is crucial to integrate the models related to the solid domain and the fluid domain of the bearing so as to acquire the geometric model for FSI heat transfer in bearings, as depicted in Figure 3.

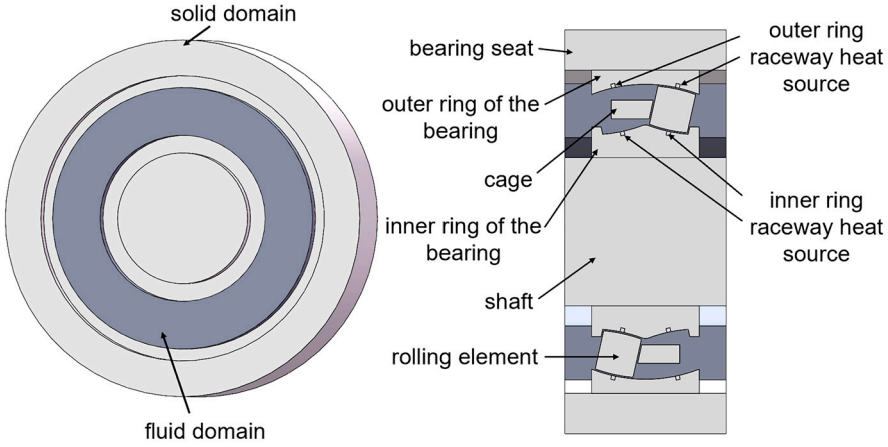


Figure 3. FSI heat transfer geometric model.

Considering the complex internal design of the bearing, and under the condition of meeting the requirements (with small calculation result errors), for the convenience

of calculation, the following simplifications and assumptions have been made for the model [29,30]:

(1) Ignore the influence of rounded corners and chamfers.
(2) Volume heat sources are added to the rolling elements, the inner raceways as well as outer raceways.
(3) To enhance the mesh's quality, a gap of 1 mm is maintained among the rolling components as well as the inner ring and the outer ring.
(4) Assume that the bearing is well-sealed and the grease will not leak. In the actual operation of the bearing, when the bearing seal ring is worn, the seal will be poor, and a small amount of grease leakage will occur.
(5) Assume that the materials involved in the model are homogeneous. In reality, there may be internal defects and uneven distribution of impurities in the materials.
(6) Ignore the possible elastic deformations of each bearing component under stress, and assume that the inner ring, outer ring, rolling elements, and cage of the bearing always remain rigid during operation. These deformations can change the contact state and friction characteristics between components.

The simplified geometric model was imported into Ansys ICEM (Version 14.5) for mesh partitioning, and the mesh was refined for the areas with added inner and outer raceway heat sources. After verifying mesh independence, the mesh number was 5,234,625. The final mesh models for FSI heat transfer and fluid domain are depicted in Figure 4.

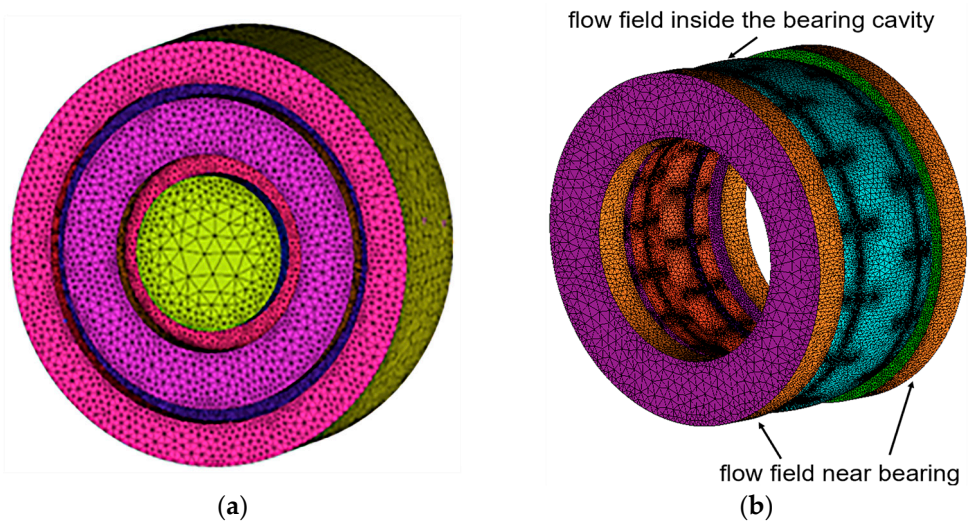


Figure 4. Bearing heat transfer mesh model. (**a**) FSI heat transfer mesh model. (**b**) Fluid domain mesh model.

2.2. Numerical Model

2.2.1. Kinematic Relationship of Bearings

Friction among the bearing components during motion leads to the generation of heat. To investigate the temperature characteristics of double-row spherical rolling bearings, it is essential to explore the operational status. Figure 5 illustrates the basic motion pattern of double-row spherical roller bearings while ignoring any elastic deformation that may occur during operation.

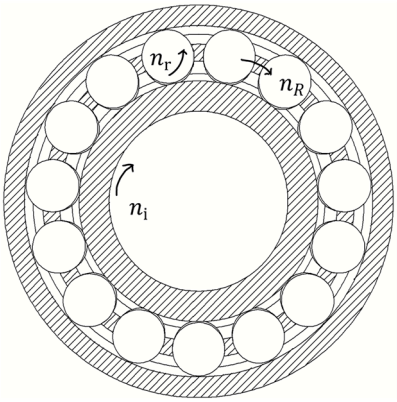


Figure 5. Bearing motion relationship.

Throughout the bearing's functioning, the bearing's inner ring has an interference mating with the shaft and rotates at the same speed as the shaft, while the outer ring stays still. The cage separates and guides the rolling elements so that the rolling elements are evenly distributed. The rolling elements and the cage rotate under the action of friction and extrusion. The movement of the cage mainly rotates following the revolution of the rolling elements. Additionally, rolling elements also undergo self-spin motion, which is a combination of rolling and sliding motion. The rotational common velocity [31] of the rolling elements, as well as the cage in double-row spherical roller bearings, is:

$$n_R = \frac{1}{2} n_i \left(1 - \frac{D_b \cos \alpha}{d_m}\right) \tag{1}$$

The rolling elements' self-spin speed [29] is:

$$n_r = \frac{1}{2D_b} d_m n_i \left(1 - \frac{D_b \cos \alpha}{d_m}\right)^2 \tag{2}$$

where n_R represents the common velocity of the rolling elements, as well as the cage (in r/min), n_r is the rolling body spin speed (in r/min), n_i represents inner ring speed (in r/min), D_b represents the rolling element diameter (in mm), α represents contact angle (in °), d_m represents the bearing pitch diameter (in mm).

2.2.2. Heat Generation Model of Bearings

While bearings operate, friction generates heat, primarily from the interaction between different components and between components and lubricating grease. Palmgen obtained the bearing's whole heat generation method [32] through experiments and analysis of the experimental results, which include the friction torque resulting from the load exerted on the bearing as well as the friction torque due to the viscous resistance associated with the lubricant, namely:

$$M = M_1 + M_2 \tag{3}$$

where M_1 and M_2, respectively, represent the friction torque owing to the bearing load and lubricant viscous resistance (in N·m).

M_1 is mainly related to the bearing's elastic hysteresis, which is largely attributable to the load and frictional losses associated with the differential sliding of the contact surfaces. This can be calculated as follows:

$$M_1 = f_1 \cdot F_1 \cdot D_m \tag{4}$$

where f_1 is a coefficient that is related to the bearing structure as well as bearing load; the range of values for double-row spherical roller bearings is 0.0004–0.0005, with the smaller value taken for light loads and the larger value taken for heavy loads. F_1 is the bearing's magnitude of the external load. When $F_a < F_r$, $F_1 = F_r$ is taken (in N), F_a and F_r are the axial and radial force. D_m is the average diameter of bearings, $D_m = 0.5\ (d + D)$ (in mm).

M_2 is primarily influenced by the kinematic viscosity of the lubricant, bearing speed, and type of bearing. The friction torque resulting from the lubricant's viscosity can be calculated as follows:

$$\begin{cases} M_2 = 1.6 \times 10^{-5} f_2 D_m^3, & v_1 n_i < 2000 \\ M_2 = 10^{-7} f_2 (v_1 n)^{\frac{2}{3}} D_m^3, & v_1 n_i \geq 2000 \end{cases} \quad (5)$$

where v_1 represents the kinematic viscosity of the lubricant at the bearing's running temperature (for grease lubrication, select the viscosity of the base oil) (in mm^2/s), n_i represents inner ring speed (in r/min), f_2 represents the parameters related to bearing type and lubricant type. For double-row spherical roller bearings lubricated with grease, the value is set to be within a range of 3.5–7.

The bearing's temperature increases due to the heat produced by the friction between its internal components. This frictional torque's heat can be calculated using Equation (6):

$$N = 1.05 \times 10^{-4} M n_i \quad (6)$$

where N is the total heat production (in kW).

2.2.3. Heat Transfer in Bearings

During operation, the bearing generates heat and transfers it to the surrounding medium, eventually reaching temperature equilibrium. There are three ways to transfer heat, which include heat conduction, heat convection, and heat radiation. In the bearing system, heat conduction [33] mainly transfers between solids, while thermal convection transfers [32] between solids and fluids. In addition, the entire bearing system undergoes thermal radiation exchange with the external space, and due to its relatively small heat exchange, it is ignored here.

This study uses the method of the common node for heat transfer between solid domains. The heat transfer method of heat conduction is relatively simple, and the heat equation is as follows:

$$Q_{cd} = G(T_2 - T_1) \quad (7)$$

where G stands for the contact thermal conductivity (in $W/(m^2 \cdot K)$). T_2 and T_1 represent the temperature of the contact surfaces between two objects (in °C).

The calculation of thermal convection is relatively complex and can be categorized into two types: free convection as well as forced convection. The relevant formulas are as follows:

$$Q_{dl} = hA\Delta t \quad (8)$$

where h and A, respectively, represent the heat transfer coefficient of convection (in $W/(m^2 \cdot °C)$) and heat transfer area of convection (in m^2). Δt stands for the temperature difference between solid and fluid (in °C).

This can be represented as follows:

$$h = \frac{Nu\lambda}{L} \quad (9)$$

The bearing seat and the outer ring are in a static state, and natural convection occurs with the surrounding air. The correlation equation is as follows:

$$Nu_s = C(GrPr)^{n_1} \tag{10}$$

$$Gr = \frac{g\alpha_1 \Delta t_1 l^3}{v^2} \tag{11}$$

$$Pr = \frac{\eta c_p}{\lambda} \tag{12}$$

In the working state, the bearing's inner ring, cage, shaft as well as air undergo forced convection. The correlation formula for convective heat transfer on the rotating cylindrical surface is:

$$Nu_t = 0.133 Re_t^{2/3} Pr^{1/3} \tag{13}$$

$$Re_t = \frac{\omega d_1^2}{v} \tag{14}$$

The coefficient of convective heat transfer between air and the rotating end face is presented as follows:

$$h_d = 0.308\lambda(m+2)^{0.5} Pr^{0.5} \left(\frac{\omega}{v_1}\right)^{0.5} \tag{15}$$

where Nu is the Nusselt number, λ is the fluid thermal conductivity (in $W{\cdot}m^{-1}{\cdot}K^{-1}$), C and n_1 are the constants obtained from experiments, L and l are the feature length (in m), Gr and Pr, respectively, represent the Grashof number and the Prandtl number, α_1 denotes the volume expansion coefficient of air (in 1/K), Δt_1 represents the temperature difference between the heat exchange surface (in °C), v is the kinematic viscosity of air (in $mm^2{\cdot}s^{-1}$), η represents the dynamic viscosity of air (in Pa·s), c_p and Re_t, respectively, represent the specific heat capacity of air (in $J{\cdot}kg^{-1}{\cdot}k^{-1}$) and the Reynolds number, ω represents the angular velocity (unit: rad/s), d_1 is the cylinder diameter (unit: mm), m is the constant representing the radial temperature distribution of a disk, m = 2.

During bearing operation, forced convection occurs between its inner surface and the fluid; this heat transfer coefficient is tough to determine. This study employs the method of establishing FSI heat transfer to create a coupled interface between the bearing's solid and fluid regions for heat transfer analysis.

2.3. Heat Allocation

The complete friction heat of the bearing is allocated to the rolling elements and inner and outer rings in the form of a volumetric heat source. Among these, the rolling elements are allocated half of the heat. The other half of the heat is allocated within the range of the inner ring and the outer ring based on their volume ratio [29].

2.4. Setting of Boundary Conditions

The FSI heat transfer mesh model was imported into ANSYS-Fluent (Version 14.5), and there was a two-phase flow of air and lubricating grease in the fluid domain. Table 2 lists the material characteristics of bearing seats, bearings, and shafts, while the physical parameters of lubricating grease and air in the fluid domain are provided in Table 3. It is assumed that air is incompressible.

Table 2. Solid domain material properties.

Name	E (GPa)	ρ (kg·m^{-3})	Poisson's Ratio	Cp (J·kg^{-1}·k^{-1})	K (W·m^{-1}·K^{-1})
Bearing seat	130	7200	0.27	510	45
Bearing	204	7810	0.3	460	46.7
Axis	210	7850	0.28	502	46.5

Table 3. Physical parameters of the fluid domain.

Name	ρ (kg·m^{-3})	ν (mm^2·s^{-1})	Cp (J·kg^{-1}·k^{-1})	K (W·m^{-1}·K^{-1})
Air	1.225	15.787	1006.4	0.0242
Grease	950	80	3600	0.0847

(1) Set the standard atmospheric pressure option in Fluent and turn on the gravity option.
(2) Based on the pressure-based solver, the VOF method was employed. In this setup, air is the main phase, while lubricating grease is the auxiliary phase. Implicit methods are configured for solving. The No. 3 lithium grease and its rheological properties were described using the Herschel–Bulkley non-Newtonian rheological model [30]. For the turbulence model, the standard k-e model is applied.
(3) The motion area utilizes a multiple reference frame model. A rotating area is defined as a motioning coordinate system, while a stationary region (outer ring) is defined as a stationary coordinate system. The speeds of the inner ring, rolling elements, as well as cage (n_R) are determined based on the bearing's kinematics part, and the fluid domain is set to the common rotational speed of the cage and rolling element.
(4) The heat source is allocated equally to the rolling elements, inner ring and outer ring, in a 1:1 ratio.
(5) The second-order upwind format is utilized to solve for the momentum, turbulent kinetic energy, turbulent dissipation rate, and energy. And the coupled algorithm is used for calculation.
(6) Enable the momentum equation, continuity equation, and energy equation, and the convergence residuals of the momentum equations along with the continuity equation and energy equation iterations are set to 10^{-3} and 10^{-6}, respectively.

3. Results and Discussion

3.1. Analysis of Temperature Field

3.1.1. Temperature Analysis of Bearing System

The numerical calculation was conducted under the following working conditions: a radial load of 214 kN, bearing speed of 1000 r/min, lubricating grease filling volume of 50%, and an ambient temperature of 26 °C. The calculated temperature field is presented in Figure 6. Subfigure (a) displays the temperature contour in the axial section, subfigure (b) displays the radial cross-section temperature contour, and subfigure (c) presents the bearing's overall temperature contour.

Figure 6a,b illustrate that the diffusion rate of heat in the fluid domain is lower than that in the solid domain. This disparity arises from the lower thermal conductivity coefficients of the air and grease located in the fluid domain relative to the counterparts of the shaft, bearings, and bearing seats in the solid domain. Additionally, the specific heat capacity of air and grease is smaller than that of the solid area, which induces the temperature to rise slowly, and the heat transfer rate is low during the heat transfer process. Because of this, the fluid domain absorbs more heat from the rolling elements, leading to an average rolling element temperature that is lower compared to that of the inner

ring. However, owing to the larger heat dissipation area between the outer ring and the outside surroundings, the average temperature of the rolling elements exceeds that of the outer ring.

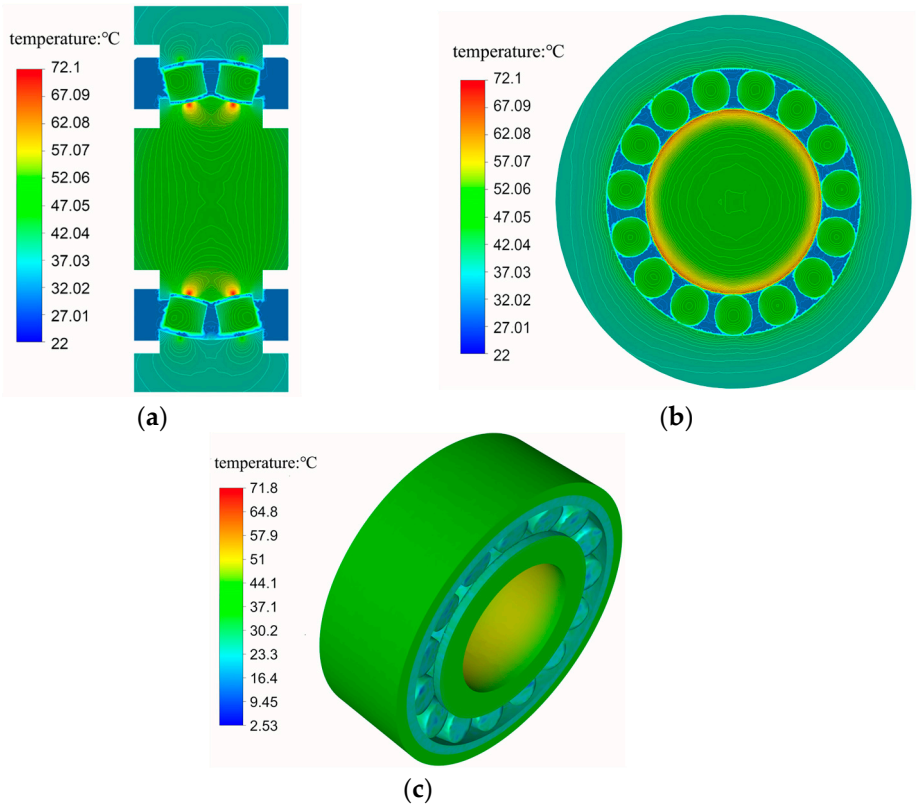


Figure 6. Bearing system temperature distribution contour. (**a**) Temperature contour in the axial section. (**b**) Temperature contour in the radial section. (**c**) Bearing's overall temperature contour.

For the relatively slow heat transfer rate in the fluid domain, the temperature gradient decreases from the center outward in rolling elements. As a result of the thermal conduction between the bearing seat and the outer ring and the heat-radiating area of the bearing seat along the heat transfer direction being greater than that of the outer ring, there is a higher thermal resistance in the outer ring [32], and the outer ring demonstrates a greater temperature gradient. In comparison with the outer ring, the bearing seat exhibits a relatively smaller ratio of heat absorption, resulting in a lower temperature gradient. Similarly, the bearing inner ring has a more pronounced temperature gradient than the shaft.

In Figure 7, the inner ring's temperature is higher compared to that of the outer ring. The temperature distribution of each part of the bearing will be analyzed from the aspects of heat generation and heat dissipation conditions. The bearing seat, which is in contact with the outer ring, has a large contact area with the outside air, as well as a substantial heat dissipation space, resulting in a lower temperature. Heat is transferred between the bearing inner ring and the shaft via thermal conduction. As a result, the shaft generates heat at a relatively fast rate. However, the contact area with the outside air is limited, which, in turn, leads to a relatively slow rate of heat dissipation. These two aspects contribute to the relatively high temperature of the bearing inner ring. The lower half of the outer ring in Figure 7a exchanges heat in a radial direction with the adjacent fluid domain, while the upper half exchanges heat with the surrounding air. Figure 7b shows that the bearing inner ring's lower half exchanges heat with air and the upper half with adjacent fluid domains in a radial direction. Notably, the specific heat capacity of air is lower than that of grease, which causes temperatures in areas containing grease to rise more slowly. As a result, there

is a relatively higher temperature between the two sides, where the outer and inner rings exchange heat with the surrounding air.

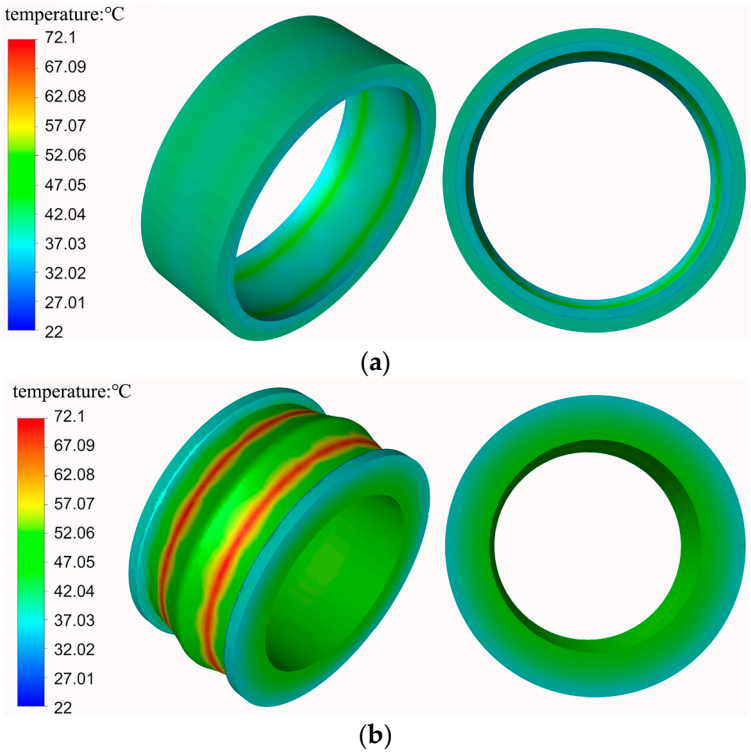


Figure 7. Temperature field between the inner ring and the outer ring. (**a**) Temperature distribution of bearing outer ring. (**b**) Temperature distribution of bearing inner ring.

From Figures 6 and 7, the temperature distribution inside the bearing shows unevenness. A higher temperature is observed in the contact surface of the rolling elements—the inner ring and the rolling elements—in the outer ring, while lower temperatures are observed in the fluid domain. The average temperatures in each area of the bearing system, ranked from highest to lowest, are as follows: inner ring (48.6 °C), shaft (45.6 °C), rolling elements (43.4 °C), fluid domain inside the bearing cavity (41.1 °C), outer ring (37.3 °C), and bearing seat (35.6 °C). The topmost temperature recorded inside the bearing is 72.1 °C, occurring in the inner ring, while the lowest temperature, 31.6 °C, is found in the fluid domain inside the bearing cavity.

The temperature of the bearing seat is the lowest for the following four reasons: (1) It has a large contact area with the surrounding air, which is conducive to heat dissipation through convection. (2) Compared to other components, the bearing seat is located externally and has smooth air circulation with the surrounding area, allowing air to flow more freely on its surface and take away heat. (3) The bearing seat does not directly generate heat but only conducts heat with the internal heat source. (4) The bearing seat is located at the outermost part, and the heat transfer path is relatively long, resulting in some loss and attenuation of heat.

The temperature differences between the inner ring, shaft, rolling elements, fluid domain inside the bearing cavity, and the outer ring and bearing seat are 13 °C, 10 °C, 7.8 °C, 5.5 °C, and 1.7 °C, respectively. From this, it can be seen that when measuring the temperature of the bearing seat to a certain value, the internal components of the bearing will have a corresponding temperature difference higher than the temperature of the bearing seat, indicating a correlation between the temperature value of the bearing seat and the temperature value of the internal components.

3.1.2. Accuracy Verification of the Computational Model

The experiment was executed through the delivery test of the jaw crusher. The operating conditions are identical to the simulation conditions. After the machine operates stably, an infrared thermometer (model DT-8500, temperature range: −50 to 500 °C, accuracy: ±2 °C) is used to measure the bearing temperature. Temperature measurement was taken on the bearing seat. The temperature measurement point is located in the middle position directly above the bearing seat, with a measurement distance of 80 cm and an emissivity of 0.9.

During the operation of the equipment, the bearing is secured to the shaft via the bearing seat. The bearing is sealed within the bearing seat, making it impossible to directly measure its internal temperature. Consequently, only the temperature of the bearing seat, which conducts heat from the bearing, can be measured. Under normal working conditions, the reliable operation of the bearing is maintained by monitoring the temperature of the bearing seat. Should the temperature of the bearing seat rise abnormally, the machine must be stopped immediately for inspection.

The comparison results of simulated temperature values and experimental temperature values at different rotational speeds are shown in Table 4, where the radial load is 214 kN, the grease filling volume is 50%, and the ambient temperature is 26 °C. In addition, the experimental temperature values presented in each group in Table 4 represent the average of three measurements taken for each condition. For instance, at a rotational speed of 1000 r/min, the experimental temperature of 37 °C is the mean of the three individual measurements (36.8 °C, 37 °C, and 37.2 °C). Furthermore, prior to each temperature measurement, the equipment was turned off and allowed to cool to ambient temperature.

Table 4. Comparison of temperature values between the simulated and experimental conditions (°C).

Speed (r/min)	Simulation Temperature (°C)	Experimental Temperature (°C)	Relative Error (%)
800	33.9	32.7 ± 0.3	3.7
1000	35.6	37 ± 0.2	3.8
1200	37.4	39 ± 0.4	4.1
1400	39.1	40.7 ± 0.2	3.9
1600	40.9	42.7 ± 0.4	4.2

For each set of experiments, upon starting the equipment each time, after it reached a stable operation state, the temperature was measured. The value-taking method was as follows: After the equipment was operating stably, the temperature was measured every 15 min three consecutive times. When the temperature readings obtained each time were the same, it indicated that the bearing had reached the thermal equilibrium state, and the reading at this time was taken as the measured value.

It can be seen from Table 4 that there is good consistency (the relative error is less than 5%) between the experimental and simulated temperature values. This outcome proves the accuracy of the developed calculation model and establishes a good basis for the subsequent bearing study. During actual operation, if the temperature of the bearing exceeds 70 °C, it should be stopped immediately to avoid bearing failure and reduce its service life.

3.2. The Correlation Between the Temperatures of the Bearing System and the Radial Loading Force

This work focuses on the impact of radial load on the temperature distribution of double-row spherical roller bearings, which are primarily subjected to radial load due to the small contact angle. The average, maximum, and minimum temperatures of each area

of the bearing system under varying radial loads are displayed in Figures 8–10, where the bearing speed is 1000 r/min, the grease filling volume is 50%, and the ambient temperature is 26 °C.

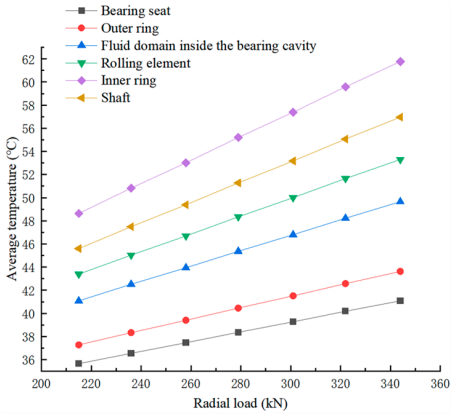


Figure 8. The impact of radial load on the average temperature of different bearing areas.

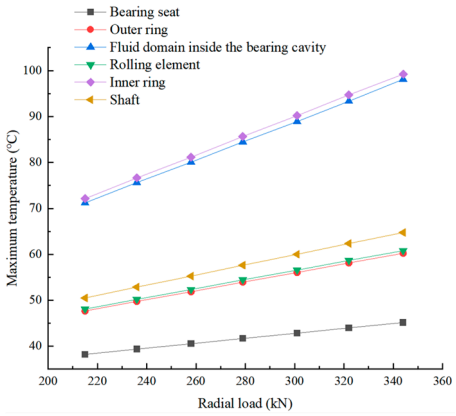


Figure 9. The impact of radial load on the maximum temperature in different areas of bearing.

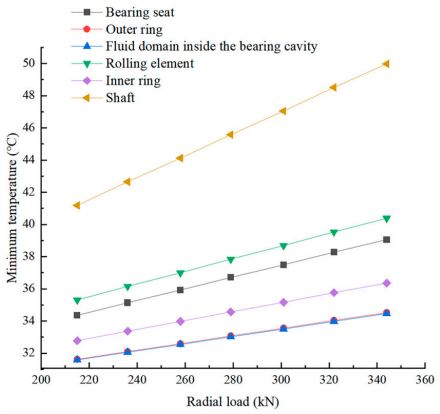


Figure 10. The impact of radial load on the minimum temperature in various areas of bearing.

As presented in Figures 8–10, as the radial load goes up, the average temperature, maximum temperature, and minimum temperature in all areas of the bearing gradually increase. This is because, as the bearing rotates, the radial load on it increases the frictional force caused by the rolling elements and the inner/outer raceways (i.e., the rolling friction), the pure sliding friction, as well as the viscous friction (between the lubricating grease), all of which increase the total heat generation within the bearing, eventually causing an increase in bearing temperature. Second, an increased radial load may cause the bearing's internal clearance and contact to become uneven. Lubricating grease will be squeezed

to both sides in the load-bearing region from the rolling element to the inner/outer ring, reducing the thickness and stability of the lubricating oil layer. This may even result in the rupture of the oil film, thereby putting the bearing in a dry or semi-dry friction state, increasing friction losses and eventually raising the temperature of the bearing.

In Figure 8, the average temperatures of the shaft, bearing, and bearing seat all show a linear increase with increasing radial load. Significant heat dissipation occurs between the bearing seat/outer ring and surrounding air due to variations in heat dissipation areas. When the load goes up, the temperature growth rate in the fluid domain of the bearing chamber, rolling elements, shaft, and inner ring gradually increases and shows a higher temperature than that of the outer ring and the bearing seat.

Figure 9 presents the highest temperatures in different areas of the bearing, sorted from the highest to lowest, which are the inner ring, the fluid domain in the bearing cavity, the shaft, the rolling element, the outer ring, and the bearing seat.

From the perspective of maximum temperature, the highest temperature is observed in the inner ring, while the fluid domain of the bearing cavity exhibits a slightly lower temperature. This is because the frictional force occurring between the inner–outer rings and the rolling elements generates the most heat. Following heat transfer and dissipation, the high-temperature area is primarily located at the interface sites of the rolling elements and the inner/outer rings of the bearing. The limited space for thermal dissipation results in the inner ring of the bearing reaching the highest temperature. Due to the FSI wall between the inner ring and the corresponding fluid domain, there is not much temperature difference at the same position. Additionally, due to heat conduction and dissipation between solids, the shaft temperature is slightly higher, followed by the rolling body, while the outer ring has a marginally lower temperature. The bearing seat has the largest area for heat dissipation to the external environment, resulting in the lowest temperature.

As illustrated in Figure 10, the lowest temperatures in diverse areas of the bearing, ranked from highest to lowest, are presented as the shaft, the rolling element, the bearing seat, the inner ring, the outer ring, and the fluid domain in the bearing cavity.

In terms of the lowest temperature, as the high-temperature areas are distributed in the contact areas between the rolling elements and the inner/outer rings, and the shaft and the inner ring conduct solid heat conduction, the temperature of the shaft is the highest and differs greatly from those of other areas. Heat is transferred between the rolling elements and the fluid domain, with the temperature of the rolling elements ranking second highest. The bearing seat conducts heat with the outer ring, and due to its larger heat dissipation area, its temperature ranks third. Due to the heat dissipation analyzed above, the temperature of the inner ring is higher than that of the outer ring. Finally, after heat exchange occurs at the interface where the outer ring couples with the fluid domain in the bearing cavity, the temperature does not differ much.

3.3. The Influence Law of Rotational Speed on the Temperature of Bearing Systems

Equation (6) shows the functional relationship between the bearing's total heat production and the revolving speed. Figures 11–13 display the average temperature, maximum temperature, and minimum temperature in all regions of the bearing system under different bearing speeds with the other simulation parameters unchanged.

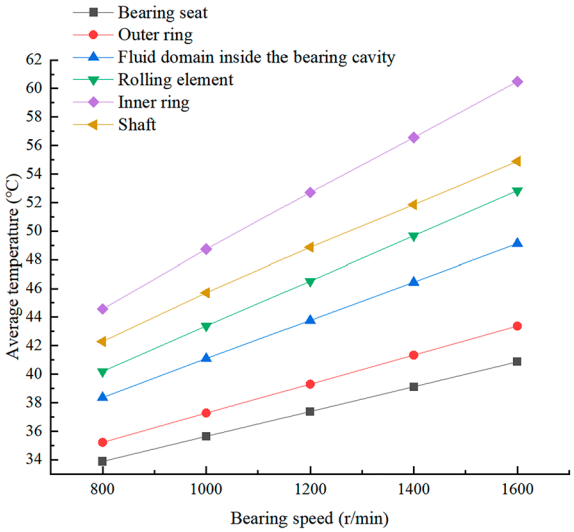


Figure 11. The influence of bearing speed on the average temperature in various areas of bearing.

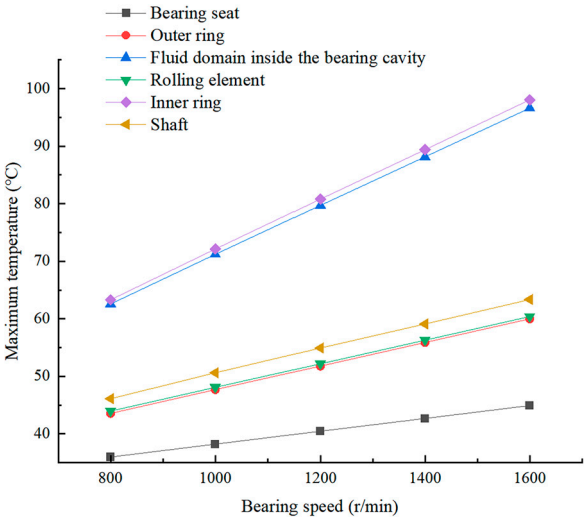


Figure 12. The influence of bearing speed on the maximum temperature in various areas of bearing.

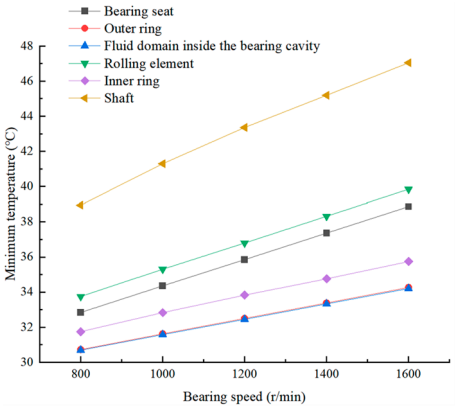


Figure 13. The influence of bearing speed on the minimum temperature in various areas of bearing.

As shown in Figures 11–13, three types of temperature in all areas within the bearing system rise along with the speed growth. This phenomenon occurs due to the intensification of the rolling friction, differential friction, and rotational friction between the rolling elements and both the inner and outer rings. Consequently, the increase in the total friction torque will lead to an increase in the heat generation inside the bearing. Additionally,

higher bearing speeds result in increased internal vibration amplitudes, causing oil film vibration. Hence, there exist some contact areas between the local rolling element and the inner/outer rings of the bearing that are not safeguarded by the lubricating oil film. The aggravated dry friction state will then generate a significant amount of heat.

As the bearing speed goes up, Figure 11 illustrates that the average temperature in each area of the bearing rises linearly, and the inner ring has the steepest slope in average temperature. This phenomenon can be attributed to the increased forced convection associated with the rotating components, coupled with the comparatively restricted convection area between the inner ring and the external environment. In contrast, the bearing seat and outer ring benefit from a larger contact area for convective heat exchange, allowing for more effective heat dissipation. Consequently, their average temperatures are lower compared to those of the fluid domain inside the bearing cavity, the rolling elements, the shaft, and the inner ring.

Figures 9 and 12 show that the distribution trend of the maximum temperature in different areas of the bearing is generally consistent. The temperature order from highest to lowest is as follows: the inner ring, the fluid domain in the bearing cavity, the shaft, the rolling element, the outer ring, and the bearing seat. Regarding the slope of the maximum temperature within each area of the bearing, it is apparent that the rotational speed imposes a more significant effect on the bearing's thermodynamic state than the radial load. This can be ascribed to the fact that as the rotational speed escalates, a more substantial quantity of heat is generated by the bearing as a whole. The explanation for the distribution tendency of the maximum temperature in every area of the bearing depicted in Figure 12 is similar to what is presented in Figure 9.

As shown in Figure 13, under the same rotational speed, the sequence of temperature from high to low is as follows: the shaft, the rolling element, the bearing seat, the inner ring, the outer ring, and the fluid domain in the bearing cavity. Comparing Figures 10 and 13 reveals that the trend of the minimum temperature change in each area of the bearing is roughly consistent. The reason is similar to Figure 10. When comparing Figures 12 and 13, concerning the temperature difference between the maximum and minimum temperatures in each area, the temperature difference between the fluid domain in the bearing cavity and the inner ring is at the largest level, with the outer ring next level, followed by the rolling element and the shaft, and the temperature of the bearing seat shows only a minor change. The reason is that the friction between the roller and the inner and outer rings is the primary factor contributing to heat generation. Although grease is capable of absorbing frictional heat effectively, it does not promote the rapid dissipation of that heat. On the other hand, solid materials demonstrate greater efficiency in quickly releasing heat.

3.4. The Influence Law of Grease Filling Volume on the Operating Temperature of Bearing System

The bearing uses No. 3 lithium grease, which is suitable for heavy-load situations. Grease is classified as a non-Newtonian fluid, and the Herschel–Bulkley non-Newtonian rheological model is employed to describe the shear motion characteristics. Upon initial injection into the bearing, a significant amount of grease is forced into the sides of the contact area, with only a small portion able to enter directly above the contact area. As the bearing operates, the grease undergoes shear action, and the base oil produced after the internal structure is damaged serves as the lubrication. The resulting lubricating oil film effectively maintains the lubrication effect on the contact surfaces among the inner parts of the bearing.

Reaching the proper filling amount of grease is crucial for the lubrication of bearings. Excessive grease filling can increase the internal shear force and viscous friction torque, which results in increased heat during operation. At the same time, the excess grease

accumulation can hinder heat dissipation and elevate the bearing temperature. Similarly, if the filling volume is insufficient and there is not enough grease to precipitate the base oil to supplement the lubricating oil film, poor bearing lubrication will happen and ultimately result in mechanical damage.

Figures 14–16 display the average temperature, maximum temperature, and minimum temperature in each zone of the bearing system under the condition that different volumes of lubricating grease are filled into the bearing system, with the other simulation parameters unchanged. When the grease filling volume ranges from 20% to 60%, the amount of grease gradually increases, and so does the amount of the base oil formed. The stable lubricating oil film can perform an excellent lubrication function, transitioning from dry friction to fluid friction. Consequently, the heat generated is significantly reduced, thereby lowering the average temperature of the bearing system. Secondly, as the lubricating fat gradually increases, it has better thermal conductivity, which can pass the heat inside the bearing to the outside faster, thereby reducing the temperature of the bearings. However, when the filling amount of lubricating grease exceeds 60%, the viscous torque between the lubricating grease increases, and the overall heat generation will increase, resulting in an overall temperature rise in the bearing system. The simulation results indicate that the optimal grease filling volume is 60%. Furthermore, as depicted in Figure 14, diverse heat dissipation situations cause the average temperature of the bearing seat and outer ring to be lower than that of the inner ring, shaft, rolling elements, and fluid domain inside the bearing.

According to Figure 15, with regard to the maximum temperature, the high-temperature zones are primarily distributed over the contact interfaces between the rolling elements and the inner/outer rings of the bearing. Among them, the temperature of the inner ring is the highest due to the friction of the rollers and the poor heat dissipation conditions. The temperature of the fluid domain inside the bearing cavity, which is coupled with the inner ring, ranks second, with only a slight difference between the maximum temperatures of the two. Additionally, heat conduction occurs between the shaft and the inner ring, resulting in the shaft temperature ranking third. When the grease filling volume ranges from 20% to 60%, the specific heat capacity of the grease is significant, resulting in a strong heat absorption capacity, leading to a higher temperature for the rolling element compared to that of the outer ring. Conversely, when the grease filling volume is set between 60% and 80%, the overall heat generation rises. The influence of heat transfer then causes the outer ring's temperature to be higher than that of the rolling element. Due to the heat dissipation condition, the temperature of the bearing seat remains the lowest.

In Figure 16, from the perspective of the lowest temperature, the shaft's temperature is the highest because it conducts heat with the inner ring. When the grease filling amount is between 20% and 60%, after heat transfer between the rolling elements and the fluid domain, the rolling elements' temperature exceeds the bearing seat's temperature. Conversely, when the grease filling volume is between 60% and 80%, the overall heat generation of the bearing increases, and the bearing seat's temperature is higher than that of the rolling elements. As the grease filling amount increases, the grease, possessing a large specific heat capacity, enhances the fluid domain's heat absorption capacity, thus leading to a gradual reduction in the temperatures of the inner ring, outer ring, and fluid domain inside the bearing cavity. The temperature drops occur rapidly at first and then slowly, stabilizing after the filling volume reaches 70%. The temperature of the outer rings and the fluid domain exhibits similar trends in the grease filling volume. Notably, the temperature curves of the bearing seat and the inner ring intersect at a filling volume of 37%, indicating an improvement in the lubrication of the inner ring at this point. Therefore, the minimum filling volume must not fall below 37%.

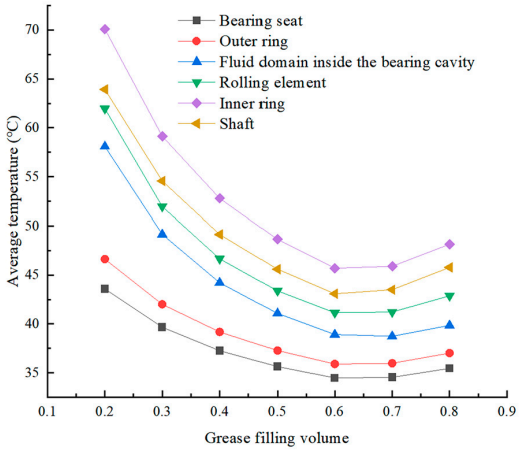


Figure 14. The influence of grease filling volume on the average temperature in various areas of bearing.

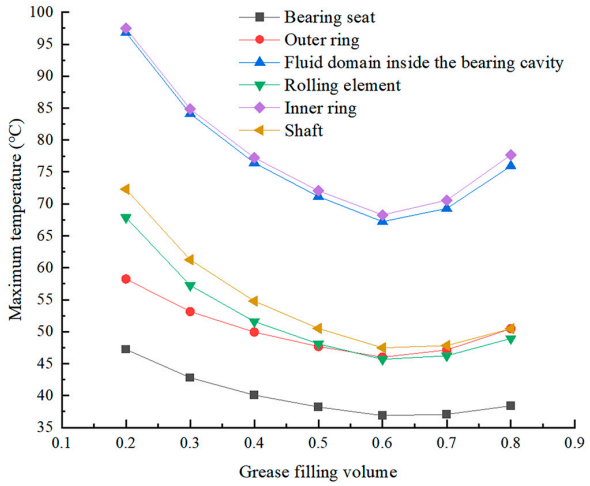


Figure 15. The effect of grease filling volume on the maximum temperature in various areas of bearing.

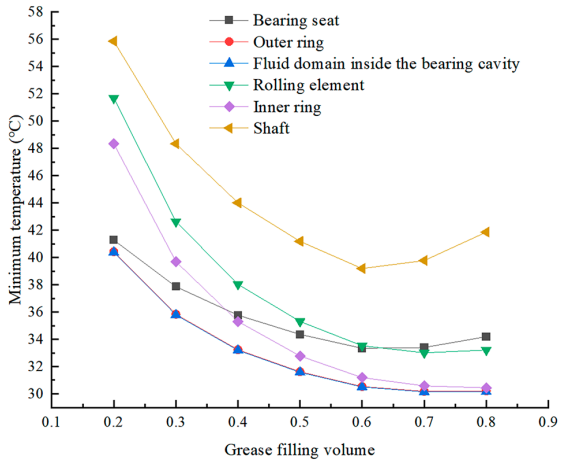


Figure 16. The effect of grease filling volume on the minimum temperature in various areas of bearing.

3.5. Discussion

(1) The accuracy of the computational model

A CFD thermal calculation model for double-row spherical roller bearings was established by employing the FSI method. After experimental verification, a relative error of 3.8% was obtained, which proved the precision of the model. Consequently, this method can be utilized to conduct optimization research on lubrication and working parameters.

(2) Working condition analysis

As illustrated in Figures 9, 10, 12 and 13, the rotation speed is more sensitive to variations in bearing temperature compared to the radial load.

When the bearing is in operation, the components inside the bearing rub against each other. The higher the rotational speed, the higher the relative motion frequency of the friction pairs between components. The amount of friction per unit of time increases significantly, generating more heat from friction. The load mainly affects the friction coefficient by changing the pressure on the contact surface. Although the friction coefficient will increase to some extent as the load increases, this increase is limited. Moreover, the change in the friction coefficient is usually not as significant as the increase in the amount of friction caused by the rotational speed.

Under high rotational speeds, the heat generated by friction accumulates rapidly, while the heat dissipation speed of the bearing is limited. The influence of the load on temperature is mainly manifested by increasing the contact pressure, which intensifies friction. However, the heat-generating effect of friction caused by the rotational speed is more remarkable, and it is more difficult to dissipate the heat in a timely manner, resulting in a more obvious temperature rise.

In scenarios where the equipment operates under high speed and heavy load, an increase in bearing temperature necessitates either a reduction in rotation speed or a replacement of the lubrication. Should the temperature continue to escalate, additional cooling measures become imperative. Conversely, if the equipment is functioning normally, it can operate effectively by maintaining appropriate load and speed. In situations characterized by low speed and light load, as long as the temperature remains within a reasonable range, an increase in equipment speed can enhance operational efficiency.

(3) The influence laws of external factors on the temperatures in each area inside the bearing

This article primarily studies the impacts of radial load, rotation speed, and grease filling volume on the average, maximum, and minimum temperatures across different areas of the bearing. The rules dictating the impact on the average temperatures in descending order within each area of the bearing are in line with the radial load, the rotational speed of the shaft, and the filling volume of the grease. The order from high to low is the inner ring, the shaft, the rolling elements, the fluid domain inside the bearing cavity, the outer ring, and the bearing seat. Notably, the temperature rise in the rolling elements, inner ring, shaft, and fluid domain inside the bearing cavity is greater than that observed in the bearing seat and outer ring.

Concerning the changing patterns of both the maximum and minimum temperatures within each area, the curves depicting the influence laws exerted by the radial load and the rotational speed exhibit a consistent tendency. This implies that the laws governing heat generation for these two factors are essentially consistent with one another. Nevertheless, when it comes to the influence law of the grease filling rate upon the temperature, notable changes emerge. The temperature curves of the various parts intersect with one another. The specific particulars will be expounded upon in the subsequent discussion.

(4) Optimal and minimum grease filling volume of the bearing system

The grease filling volume exerts significance on the bearing temperature. Under simulated conditions, it has been determined that the lubricating effect is the best when the grease filling volume is 60%. When the grease filling volume lies within a range of 20% to 60%, the temperature fluctuation amplitude across various areas of the bearing drops swiftly. Nevertheless, once the filling volume surpasses 60%, the average temperature in each zone of the bearing starts to ascend.

Simultaneously, only when the grease filling volume exceeds 37% can effective lubrication of the inner ring by the bearing be accomplished. This value can be regarded as the essential lower bound for the lubricating grease, serving as an alarm reference in practical applications.

(5) Application prospects

The temperature data of the bearing, derived from the CFD numerical calculations presented in this study, can serve as a reference for the bearing's operational temperature in real-world applications. Furthermore, the methodology employed to analyze the temperature characteristics of the bearing can be adapted for other bearing studies by modifying the model structure and boundary conditions. This research holds substantial significance for the fields of tribology and bearing applications.

4. Conclusions

By developing CFD thermal calculation models of the bearing system under grease lubrication in the ANSYS-Fluent module, numerical simulations were performed on various parts of the double-row spherical roller bearing system to obtain the temperature distribution. Then, an analysis was conducted on the temperature characteristics of the bearings under different working conditions, leading to the following conclusions:

(1) The relative error of the FSI heat transfer model of the bearing is less than 5%, which indicates high accuracy. Consequently, this model holds great potential for being utilized in further optimization studies.
(2) The rotation speed is more sensitive to bearing temperature. During the equipment's operation, if the temperature exceeds safe levels, it is advisable to first adjust the rotation speed to maintain normal equipment functioning.
(3) Under the specific working conditions with a radial load of 214 kN, a bearing rotational speed of 1000 r/min, and an ambient temperature of 26 °C, the bearing system can achieve its optimal operation when the optimal grease filling volume reaches 60%. This is consistent with the usual requirement that the filling rate should be approximately two-thirds.

In summary, the FSI heat transfer method was employed to conduct a CFD simulation of the double-row spherical roller bearing, enabling a detailed analysis of the temperature distribution across various areas of the bearing, which can provide valuable insights for practical applications. However, it is crucial to note that the fluid–solid coupling heat transfer problem addressed using Fluent is a single-phase fluid–solid coupling scenario. At the coupling interface, the data transfer is unidirectional: the CFD calculation results (such as temperature) are transferred to the solid structure analysis, while the influence of the solid on the fluid is considered to be negligible. Consequently, the effects of radial load on bearing displacement and deformation, which would require a bidirectional fluid–solid coupling heat transfer approach, were not considered in this study. The research team intends to further investigate the issue of two-way fluid–solid coupling heat transfer in future research to enhance simulation accuracy.

Author Contributions: Conceptualization, C.F. and T.C.; methodology, C.F. and T.C.; software, T.C., H.L. and H.C.; validation, C.F., T.C., Y.L. and W.H.; formal analysis, T.C., C.F. and Y.Z.; investigation, T.C. and H.Y.; resources, H.Y. and C.F.; data curation, T.C. and Y.Z.; writing—original draft preparation, T.C.; writing—review and editing, H.Y., C.F. and H.L.; visualization, T.C., H.L. and H.C.; supervision, Y.Z., Y.L. and W.H.; project administration, C.F. and H.Y.; funding acquisition, Y.Z., H.Y. and C.F. All authors have read and agreed to the published version of the manuscript.

Funding: This research was funded by the Science and Technology Project of Henan Province (Grant No. 242102320150) and Joint Funds of the National Natural Science Foundation of China (Grant No. 52301205).

Data Availability Statement: The data that support the findings of this study are available from the corresponding authors upon reasonable request.

Conflicts of Interest: The authors declare no potential conflicts of interest.

References

1. Chen, K.; Li, X.L.; Jin, X.Y.; Guo, F.; Gerhard, P. Bench Test of Grease-Lubricated Rolling Bearing Performance Under Different Ambient Temperatures. *Bear* **2024**, *5*, 44–50.
2. Chang, Z.; Jia, Q.; Yuan, X.; Chen, Y.L. Main failure mode of oil-air lubricated rolling bearing installed in high speed machining. *Tribol. Int.* **2017**, *112*, 68–74. [CrossRef]
3. Xue, K.; Wang, X. Correlation Between Oxidation Failure of Bearing Grease and Rolling Wear. *Synth. Lubr.* **2022**, *49*, 15–20.
4. Yang, F.L. Research on Temperature Field and Grease Degradation Mechanism of High-Speed Locomotive Axle Box Bearing. Master's Thesis, Henan University of Science and Technology, Luoyang, China, 2022.
5. Allmaier, H. Increase Service Life for Rail Wheel Bearings—A Review of Grease Lubrication for This Application. *Lubricants* **2022**, *10*, 36. [CrossRef]
6. Jia, C.H.; Chen, G.C.; Wang, Y.S.; Wang, G.F.; Fan, Y.Q. Thermal Analysis of Double Row Tapered Roller Main Bearings for Wind Turbines. *Bear* **2023**, *6*, 43–58.
7. Yang, F.L.; Li, X.; Deng, S.E.; Zhang, W.H.; Wang, S.M. Analysis on Temperature Field in Axle Box Bearings of High Speed Locomotive. *Bear* **2020**, *12*, 1–6.
8. Chen, C.Y.; Li, J.S.; Yu, Y.J.; Xue, Y.J. Study on Temperature Rise Characteristics of High Speed Angular Contact Ball Bearings in Oil-Air Lubrication. *Mach. Des. Manuf.* **2021**, *9*, 216–221.
9. Xu, H.H.; Jiang, X.J.; Jiang, J.L. Simulation Analysis on the Thermometer Hole and Bearing Parts Temperature Field for the High Speed Train. *Comput. Simul.* **2021**, *38*, 134–137.
10. Sun, J.L.; Guo, H.S.; Guo, X.; Ma, C.; Peng, Y. The Simulation Analysis and Experimental Study on the Temperature Field of Four Row Rolling Bearing of Rolling Mill under Non-Uniform Load Conditions. *Sensors* **2024**, *24*, 914. [CrossRef] [PubMed]
11. Cabezas, S.; Hegedus, G.; Bencs, P. A New Thermal Model of an Angular Contact Ball Bearing, in a Standard Arrangement, subjected to Radial Loads, Based on State Variables and Control Volumes. *Acta Polytech. Hung.* **2024**, *21*, 147–164. [CrossRef]
12. Gao, S.Z.; Wang, Y.J.; Zhang, Y.M. Thermal behavior study and experimental testing of deep groove ball bearing. *J. Mech. Sci. Technol.* **2023**, *37*, 6676–6689. [CrossRef]
13. Wang, B.S.; Liu, Y.; Zhang, B.; Huai, W.Q. Analysis of the Temperature Characteristics of High-speed Train Bearings Based on a Dynamics Model and Thermal Network Method. *Chin. J. Mech. Eng.* **2022**, *35*, 104. [CrossRef]
14. Zhang, G.T.; Su, B.; Liu, F.B.; Zhang, W.H.; Yang, H.S. Thermal Analysis Based on Dynamic Performance of Rocker Arm Full-Type Needle Bearings. *Lubricants* **2022**, *10*, 104. [CrossRef]
15. Li, F.; Cai, J.B.; Qiu, W.B.; Wang, K.; Pan, Z. Simulation and Analysis of Temperature Field of Self-aligning Roller Bearing. *Modul. Mach. Tool Autom. Manuf. Tech.* **2020**, *11*, 131–134.
16. Zhang, Y.M.; Zhou, T.Y.; Ji, S.T.; Zhang, H. Simulation and Experimental Analysis of Working Temperature Field of Needle Roller Bearing. *Modul. Mach. Tool Autom. Manuf. Tech.* **2021**, *11*, 156–159.
17. Chen, Y.L.; Li, J.W. Heat Generation and Temperature Field Simulation Analysis of High Speed Angular Contact Ball Bearing of Spacecraft. *Mach. Tool Hydraul.* **2020**, *48*, 167–170.
18. Gao, S.Z.; Wang, Y.J.; Zhang, Y.M.; Yu, C.H. Simulation analysis of frictional heat and temperature field of deep groove ball bearings. *Mach. Des. Manuf.* **2024**, 1–5. [CrossRef]
19. Li, X.P.; Xue, Y.J.; Si, D.H.; Jiang, S.F.; Ma, X.Q. Study on the Temperature Rise of Angular Contact Ball Bearings Under Ring Lubrication. *Modul. Mach. Tool Autom. Manuf. Tech.* **2019**, *3*, 40–43.
20. Sun, J.; Fang, X.; Yao, J.M.; Zhang, Z.; Guan, R.Y.; Zhang, G.X. Thermal characteristics and distribution rule of lubrication film of full ceramic ball bearing under different service condition. *Ind. Lubr. Tribol.* **2023**, *75*, 919–932. [CrossRef]

21. Li, M.M.; Wang, Y.; Chen, W.F.; Zhu, R.P. Temperature rise characteristics for angular-contact ball bearings with oil-air lubrication based on fluid-solid conjugate heat transfer. *Adv. Mech. Eng.* **2021**, *13*, 1–13. [CrossRef]
22. Li, J.N.; Xue, J.F.; Ma, Z.T. Study on the Thermal Distribution Characteristics of High-Speed and Light-Load Rolling Bearing Considering Skidding. *Appl. Sci.* **2018**, *8*, 1593. [CrossRef]
23. Sun, Q.G.; Wang, Y.F.; Wang, Y.; Niu, P.; Wang, X.S. Numerical Study on Rolling Bearing Temperature Field Under the Oil-air Lubrication. *Appl. Mech. Mater.* **2014**, *487*, 580–584. [CrossRef]
24. Ma, X.Q.; Zhang, M.; Yang, F.; Xue, Y.J.; Gu, R.J.; Guo, N. Analysis of Circulation Characteristics and Heat Balance of High-Speed Rolling Bearing under Oil-Air Lubrication. *Lubricants* **2023**, *11*, 136. [CrossRef]
25. Jiao, Y.H.; Li, X.M.; Liu, M.Y.; Guo, F. Experimental study on oil-air lubrication parameters for bearing units. *Bear* **2018**, *11*, 43–47.
26. Li, Y.J.; Yang, F.; Liu, Z.X.; Zhang, C.Y.; Lu, Y.G. Flow and thermal analysis of oil air two-phase medium in bearing chamber. *J. Aerosp. Power* **2021**, *36*, 606–615.
27. Zhang, Y.Y.; Ni, A.G.; Ma, C.B.; Xu, T.; Chen, S.J.; Sun, J.J. Fluid-Solid Coupled Heat Transfer Characteristics of High-Speed Ball Bearings with Under-Race Lubrication. *Tribology* **2024**, 1–17. Available online: https://link.cnki.net/urlid/62.1095.O4.20240929.1539.008 (accessed on 13 February 2025).
28. Guo, L.; Li, B.; Zhang, Z. Simulating Temperature Field and Thermal Deformation of Liquid Dynamic and Static Pressure Bearing. *Mech. Sci. Technol. Aerosp. Eng.* **2014**, *36*, 606–615.
29. Zhang, R. Investigation on the Two-Phase Flow and Heat Transfer Inside High-Speed Ball Bearings for in Vehicular Transmission. Master's Thesis, Beijing Institute of Technology, Beijing, China, 2016.
30. Sun, C.D. Analysis of Grease Flow and Thermal Characteristics in Grease Lubricated High-Speed Angular Contact Ball Bearing Cavity. Master's Thesis, Lanzhou University of Technology, Lanzhou, China, 2018.
31. Cheng, Z.X. The Research on the Movement Law of Wind Turbine Bearing Lubricating Grease and The Grease Change. Master's Thesis, North China University of Water Resources and Electric Power, Zhengzhou, China, 2021.
32. Li, C. Analysis of Temperature Characteristics of Wind Turbine Spindle Bearing. *Mech. Res. Appl.* **2022**, *35*, 8–12.
33. Wang, Z. Analysis of Oil-Air Lubrication Two-Phase Heat Flow Coupling Characteristics of High Speed Angular Contact Ball Bearing. Master's Thesis, Lanzhou University of Technology, Lanzhou, China, 2020.

Disclaimer/Publisher's Note: The statements, opinions and data contained in all publications are solely those of the individual author(s) and contributor(s) and not of MDPI and/or the editor(s). MDPI and/or the editor(s) disclaim responsibility for any injury to people or property resulting from any ideas, methods, instructions or products referred to in the content.